AD-A121 695 SIZE DISTRIBUTIONS OF PYROTECHNICALLY GENERATED HYGROSCOPIC AEROSOLS(U) NAVAL RESEARCH LAB WASHINGTON DC W A HOPPEL ET AL. 19 NOV 82 NRL-MR-4946 1/1

UNCLASSIFIED SBI-AD-E000 512 F/G 17/4 NL

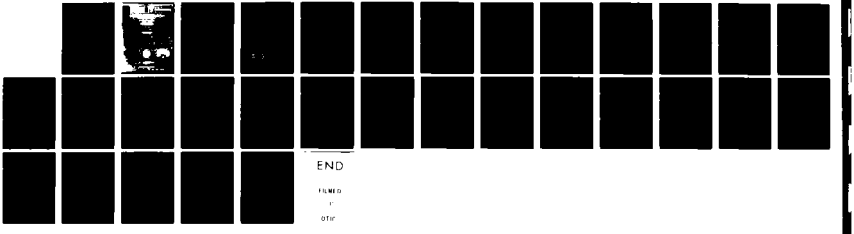

END

FILMED

DTIC

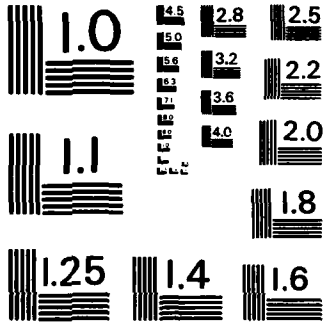

MICROCOPY RESOLUTION TEST CHART
NATIONAL BUREAU OF STANDARDS-1963-A

SECURITY CLASSIFICATION OF THIS PAGE (When Data Entered)

REPORT DOCUMENTATION PAGE		READ INSTRUCTIONS BEFORE COMPLETING FORM
1. REPORT NUMBER NRL Memorandum Report 4946	2. GOVT ACCESSION NO. AD-A121615	3. RECIPIENT'S CATALOG NUMBER
4. TITLE (and Subtitle) SIZE DISTRIBUTIONS OF PYROTECHNICALLY GENERATED HYGROSCOPIC AEROSOLS		5. TYPE OF REPORT & PERIOD COVERED Interim report on a continuing NRL problem. 6. PERFORMING ORG. REPORT NUMBER
7. AUTHOR(s) W.A. Hoppel and G.M. Frick		8. CONTRACT OR GRANT NUMBER(s)
9. PERFORMING ORGANIZATION NAME AND ADDRESS Naval Research Laboratory Washington, D.C. 20375		10. PROGRAM ELEMENT, PROJECT, TASK AREA & WORK UNIT NUMBERS 61153N; WR02402002; 43-1114-0
11. CONTROLLING OFFICE NAME AND ADDRESS Naval Air Systems Command Washington, D.C. 20361		12. REPORT DATE November 19, 1982 13. NUMBER OF PAGES 30
14. MONITORING AGENCY NAME & ADDRESS(if different from Controlling Office)		15. SECURITY CLASS. (of this report) UNCLASSIFIED 15a. DECLASSIFICATION/DOWNGRADING SCHEDULE

16. DISTRIBUTION STATEMENT (of this Report)

Approved for public release; distribution unlimited.

17. DISTRIBUTION STATEMENT (of the abstract entered in Block 20, if different from Report)

18. SUPPLEMENTARY NOTES

19. KEY WORDS (Continue on reverse side if necessary and identify by block number)

Hygroscopic aerosols	Aerosol size distribution
Optical countermeasures	Alkali-Halide smokes
Artificial smoke and haze	Pyrotechnically generated

20. ABSTRACT (Continue on reverse side if necessary and identify by block number)

Measurements of the size distribution and solubility were made on pyrotechnically generated, alkali-halide smokes in Calspan Corporation's 600 cubic meter environmental chamber. Detailed size distributions are presented and show that the mean size increased as the payload increased. A discussion of the aerosol formation process and growth of particles by recondensation of pyrotechnic material is also presented.

DD FORM 1 JAN 73 1473 EDITION OF 1 NOV 65 IS OBSOLETE
S/N 0102-014-6601

SECURITY CLASSIFICATION OF THIS PAGE (When Data Entered)

CONTENTS

SIZE DISTRIBUTIONS OF PYROTECHNICALLY GENERATED HYGROSCOPIC AEROSOLS

I. BACKGROUND

The objective of the NAVAIR artificial aerosol program is to develop an effective screening agent for visible and infrared regions of the E-M spectrum utilizing pyrotechnically generated hygroscopic (soluble) aerosols. The purpose of using hygroscopic aerosols is to take advantage of the high humidity environment in which the Navy operates. Over the open oceans hygroscopic particles will grow by absorption of water vapor such that the mass of the terminal aerosol is greatly increased over that which can be obtained by burning the same payload of nonhygroscopic material.

One aspect of the program has been the evaluation of aerosols generated by different pyrotechnic formulations developed at the Naval Weapons Center. These were burned in Calspan's 600 m^3 chamber to determine the relative merits of different formulations. Some results of previous tests are given by Hanley et al. (1980, 1981). NRL participated in the 1982 tests using several unique instruments developed at NRL for making measurements of the size distribution and solubility of natural atmospheric aerosols (Hoppel, 1981). The purpose of this report is to give the results obtained by NRL during the March 1982 measurements in Calspan's chamber. Only NRL results are given here; a more complete description of Calspan's chamber and the results of concurrent measurements made by Calspan of optical and infrared extinction, mass yield measurements, and the effect of relative humidity on extinction are given in a separate Calspan report (Hanley et al 1982).

II. Growth of Hygroscopic Particles with Increasing Relative Humidity: Theory

The relationship between the saturation ratio S (relative humidity divided by 100) and the equilibrium radius r of a particle of dry radius r_d is given by

$$S = \text{EXP}\left(\frac{A}{r}\right) \cdot \text{EXP}\left[\frac{-\eta B^o}{\eta^o\left(\frac{r^3}{r_d{}^3} - 1\right)}\right] \qquad (1)$$

where the first factor accounts for the change in vapor pressure due to the surface tension σ and the second factor the reduction of vapor pressure due to the solute effect (Raoult's Law).

$$A = \frac{2\sigma}{\rho_w R_v T} \approx 4.33\text{X}10^{-7}\ \frac{\sigma_w}{T}$$

Manuscript approved October 1, 1982.

where σ_w is the surface tension of water, ρ_w is the density of water, R_v is the specific gas constant of water vapor and T is the temperature. η is the exponential mass increase coefficient given by

$$\eta = \frac{\bar{\nu}\,\bar{\phi}\,\varepsilon\,\gamma\,M_w}{\bar{M}_s}$$

where $\bar{\nu}$ is the mean number of moles of ions and undissociated molecules per mole of salt mixture; $\bar{\phi}$ is the observed practical osmotic coefficient; $\bar{M}$ is the mean molecular weight of the salt mixture; ε is the mass fraction of soluble material in the particle; M_w is the molecular weight of water; and γ is a correction factor taking into account adsorption (or desorption) of ions at the solid-solution interface. η^o is the mass increase coefficient for an infinitely dilute solution, and

$$B^o \equiv \frac{\rho_o\,\eta^o}{\rho_w}$$

where ρ_o and ρ_w are the densities of the dry particle and water respectively. We define B^o as the aerosol hygroscopicity parameter. The reason for formulating Eq. (1) in terms of B^o will become clearer later when we show that B^o can be determined experimentally. For details of this formulation see Fitzgerald et al. (1982).

For dilute solutions as is the case for hygroscopic particles in equilibrium with an environment of 100% RH, Eq. (1) can be simplified to

$$S = 1 + \frac{A}{r} - \frac{\eta\,B^o}{\eta^o}\,\frac{r_d^3}{r^3} \qquad (2)$$

At S = 1 (100% RH) Eq. (2) can be written as

$$B^o = \frac{\eta^o}{\eta_{100}}\,\frac{A\,r_{100}^2}{r_d^3} \qquad (3)$$

The ratio η^o/η_{100} never differs greatly from unity for various compositions of interest whereas B^o depends strongly on the activity of the solute and the fraction of soluble material. In our calculations η/η^o was assigned the value of 0.85; see Fitzgerald et al. (1982).

The important thing to notice from Eq. (3) is that the parameter B^o can be determined by measuring the dry radius r_d and the equilibrium radius at exactly 100% RH. The instrumentation and procedures by which r_d and r_{100} can be measured are described in the next section.

Once B^o is determined experimentally it can be substituted back into Eq. (1) and the functional dependence between radius r and relative humidity RH can be determined. Later it will be shown that the values of B^o for the pyrotechniques examined were in the range of about 0.3 to 0.4. Figure 1, shows the relationship between the ratio r/r_d and relative humidity for a dry size particle of 0.1 μm for several values of B^o. The ratio r/r_o depends upon the dry size r_d but this dependence is very weak when the particles are larger than about 0.1 μm radius, as is shown in Figure 2.

The relative mass increase is proportional to the volume increase or cube of the radius. Figure 3 illustrates the relative increase in mass of hygroscopic particles with various solubilities over what would be obtained if the aerosol were nonhygroscopic ($r/r_d = 1$).

III. INSTRUMENTATION

The primary measurements made by NRL during these tests were aerosol size distributions and particle growth.

Size Distribution. Many combustion processes produce large numbers of small particles (< 0.1 μm) and there were some indications from previous experiments that small particles existed in Calspan's chamber after the burning of pyrotechnics. Such small particles were not found in reduced scale experiments at NRL where pyrotechnics were burned in a bell jar and ventilated directly into a metalized mylar storage bag before size distribution measurements were obtained (Hoppel 1981). One of the objectives of NRL's participation in the 1982 Calspan experiments was to make precise measurements of the size distribution in the size range down to 0.01 μm radius, to see if a significant amount of mass was generated in the particle size range smaller than that which would contribute to light scattering. The NRL-developed differential mobility analyzer is an excellent instrument for the sizing of particles in the size range 0.006 to 0.5 μm radius. The measurement scheme for the mobility analyzer is as follows: The aerosol sample is brought to charge equilibrium (Boltzmann distribution) by passing it through a region of bipolar ionization. Aerosol particles in a narrow mobility range are selectively segregated and transmitted to a continuous flow cloud chamber where the number transmitted is counted. The mobility distribution of aerosols is determined from the number of particles transmitted as a function of the polarizing voltage. Knowledge of the charge and mobility distributions is sufficient for the reconstruction of the size distribution. The details of the instrument and the particle detector can be found in previous papers; (Hoppel 1978, 1981).

Optical particle size spectrometers can be used for sizing aerosol particles larger than a few tenths of a micron. Two such instruments were taken to Calspan. One was the Particle Measuring System ASASP which failed the first day in operation; the other was a Royco Model 225.

The sizing instrumentation was designed for atmospheric measurements where the aerosol concentrations are much lower than those which occurred in the chamber after burning the pyrotechnic. Only when the payload burned was half a gram or less could the instrumentation be used without dilution of the sample. A dilution system had been designed prior to the experiments and provided dilutions up to one part sample to 140 parts filtered air, however the higher the dilution ratio the less accurately was it known. Also,

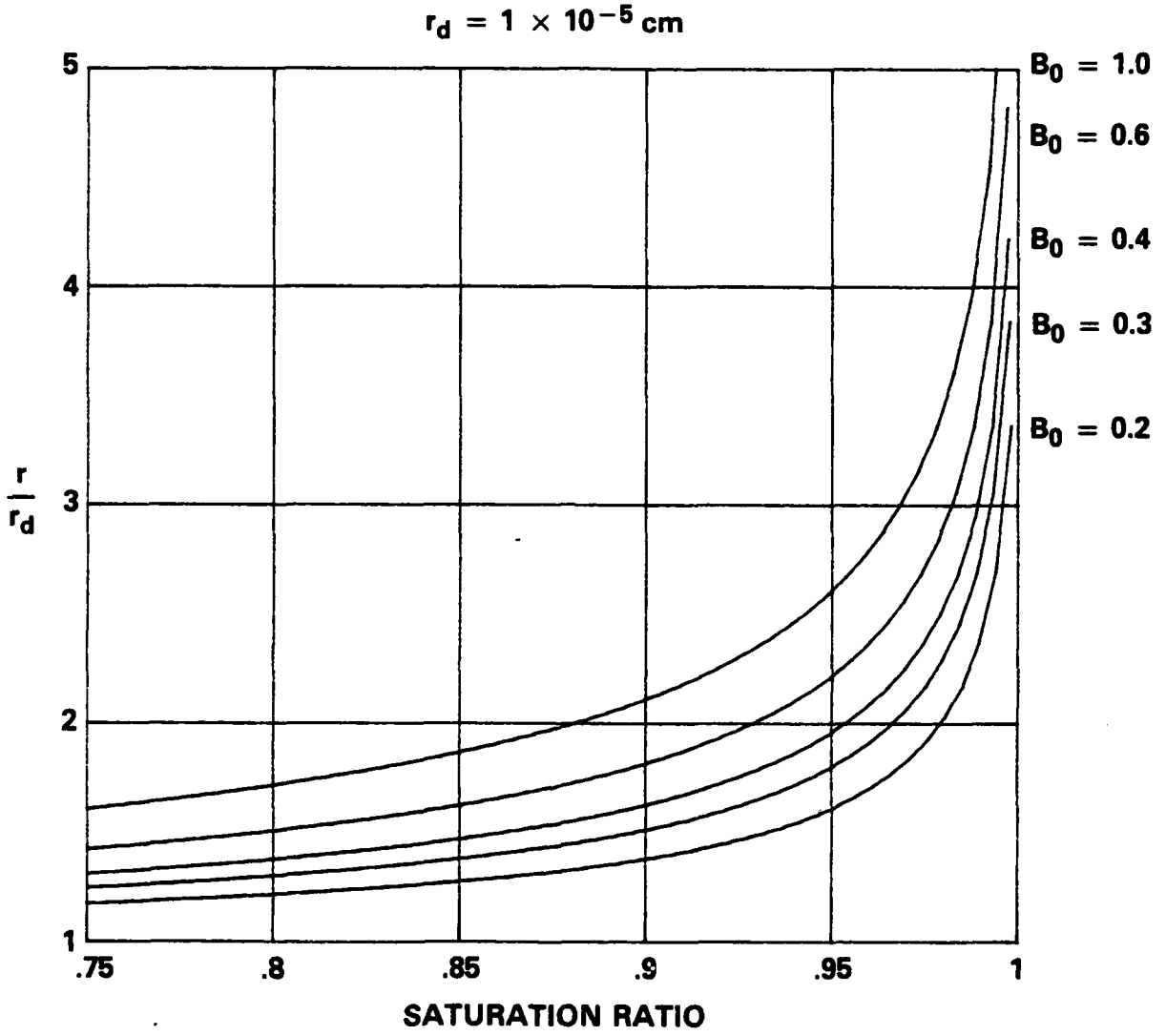

Fig. 1 — The dependence of equilibrium particle size on relative humidity and solubility for particles with dry radius of 0.1 micron

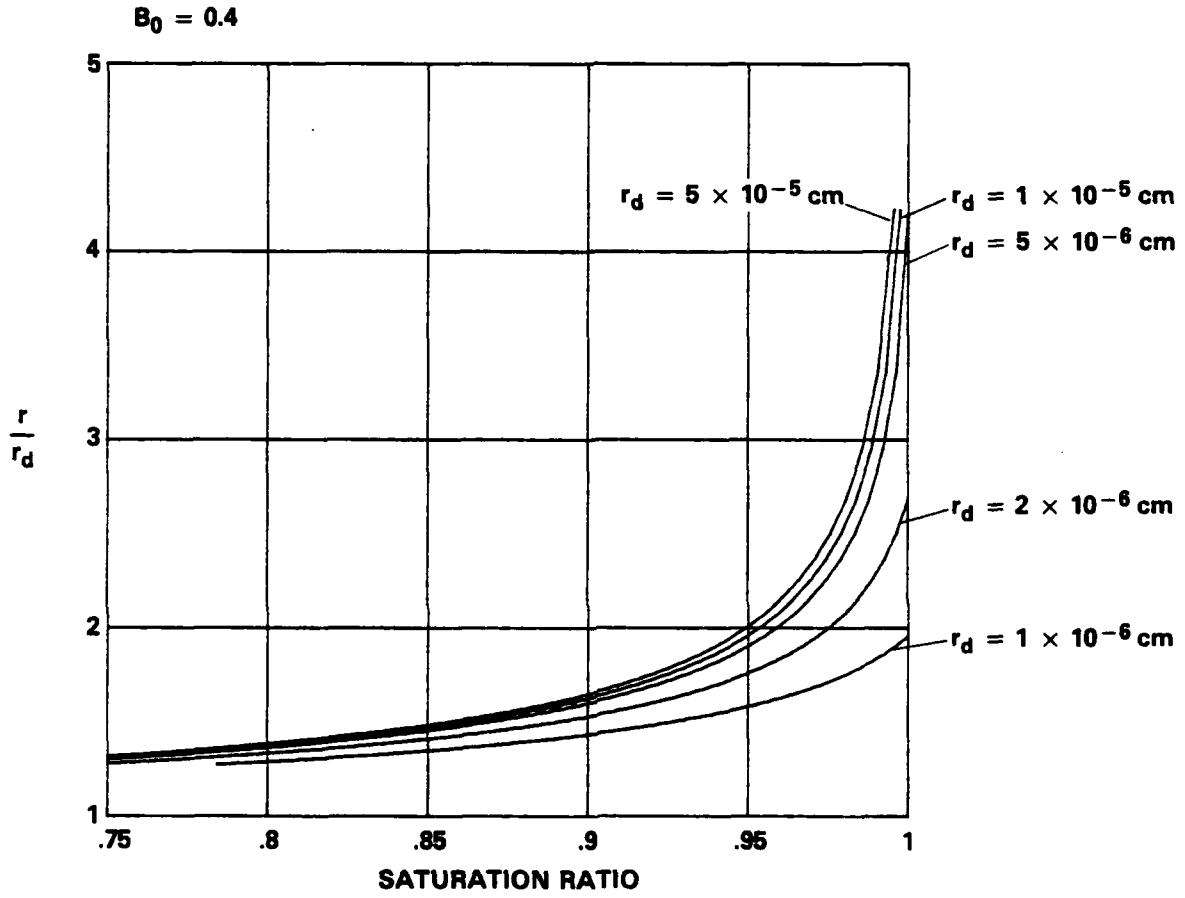

Fig. 2 – The dependence of equilibrium particle size on relative humidity and dry radius for the solubility $B_o = 0.4$

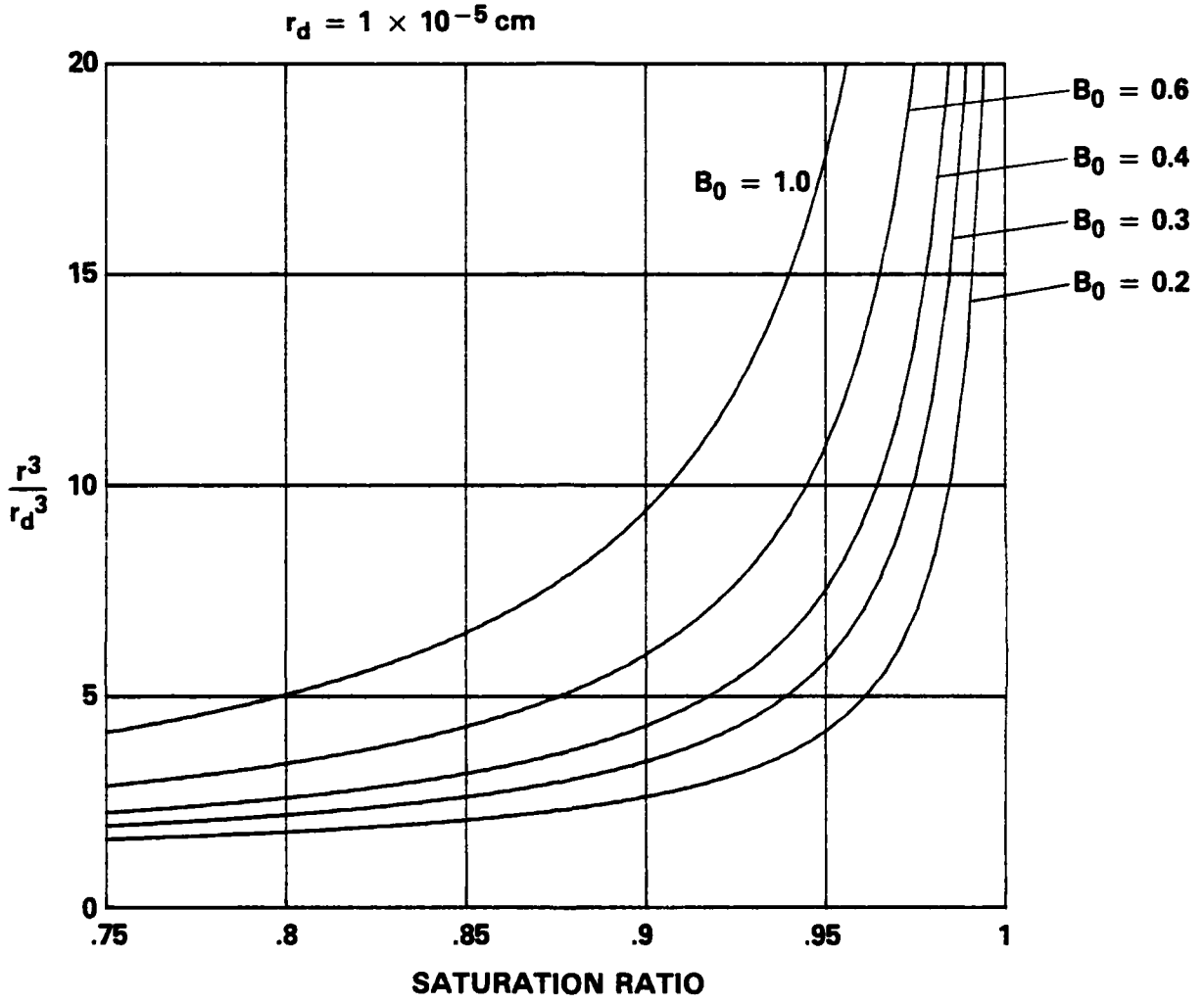

Fig. 3 – The dependence of particle volume and relative humidity and solubility of particles with 0.1 micron dry radius

there was probably significant loss of larger particles ($r > 3$ μm) in the diluter itself. On several occasions when data was taken at two dilution ratios for the same sample, the corrected counts would disagree by up to 40%. This uncertainty in the absolute calibration of the dilution system does not affect the shape of the size distribution, but only its magnitude. Since the absolute magnitude of the concentration is in doubt the size (or mass) distribution should not be used to calculate absolute yields, however, they can be used to characterize the size distributions produced by various burns.

Measurement of Particle Growth at 100% Relative Humidity. In the last section the theory which relates the growth of a particle with increasing humidity to its composition was given. It was shown (Eq. (3)) that the hygroscopicity parameter B^o could be determined by measuring the dry radius of a particle and its size at 100% RH. This measurement is made using the mobility analyzer in conjunction with the NRL isothermal haze chamber (IHC) (Hoppel, 1981).

The dry aerosol is first introduced into the mobility analyzer where particles of a well defined mobility are stripped off and transmitted to the IHC. The IHC is a chamber where the sample is brought to 100% RH and the residence time in the chamber is sufficient for the particles to reach their equilibrium size at 100% RH (provided the particles are small enough so that their equilibrium size is less than 3 μm radius). The size distribution of the enlarged particles is measured as they exit from the IHC with a Royco Optical Particle Size Spectrometer. Results of this type measurement are given in the next section (see Figure 10). Once the dry size and size at 100% RH is determined these values are substituted into Eq. (3) and the hygroscopicity factor B^o is determined.

IV. RESULTS

A number of tests were carried out in Calspan's environmental chamber between 10 and 18 March 1982. A list of the experiments in which NRL obtained useful data is shown in Table I. Calspan has presented their data in terms of Test Numbers which are also given in the Table for purposes of cross reference.

As with any experiment where multiple measurements are made, the optimum procedure for one measurement is seldom the best procedure for another. For IR extinction and mass loading experiments, large payloads were required whereas for the size distribution measurements low concentrations were desirable. During the first four days (9 to 12 March) high priority was given to Calspan's IR extinction and mass loading measurements at several humidities. During the later part of the experiment (13 to 17 March) the emphasis was on the NRL size distribution data.

The typical procedure was to flush the chamber for several hours with filtered outside air until virtually all particles were removed. The warming of the winter air upon entering the chamber resulted in a relative humidity below 40% in the chamber unless the air was purposely humidified. Humidification was applied on 11 and 12 March and was important for the extinction and mass loading measurements. The data taken during these two days by NRL is not reported here because the relative humidity to which of the NRL measurements corresponded is not known. (The relative humidity in the chamber was known but the relative humidity in our instruments which were outside the chamber proper

TABLE I: SUMMARY OF EXPERIMENTS

Date 1982	Pyrotechnic	Payload Size	Aerosol Size Distribution	Solubility Data	Calspan Test Number
March 10	CY85A	0.5 g	Yes (2)	No	2
	CY85A	160 g	Yes (3)	No	2
	LiCl	0.5 g	Yes (2)	No	3
	LiCl	80 g	Yes (2)	No	3
March 13	CY85A	0.5 g	Yes (2)	Yes	7
	CY85A	5.0 g	Yes (2)	Yes	7
	LiCl	0.5 g	Yes (2)	Yes	8
	LiCl	5.0 g	Yes (1)	No	8
March 15	NWC-164	0.5 g	Yes (2)	Yes	9
	NWC-164	5.0 g	Yes (2)	No	9
	LiCl	0.5 g	Yes (2)	Yes	10
	LiCl	5.0 g	Yes (2)	No	10
March 16	NWC-79	0.5 g	Yes (2)	No	11
	NWC-79	5.0 g	Yes (2)	Yes	11
	NWC-78	0.5 g	Yes (2)	Yes	12
	NWC-78	5.0 g	Yes (3)	No	12
March 17 Ventilated	CY85A	0.5 g	Yes (2)	No	13
	CY85A	5.0 g	Yes (2)	No	13
Chimney	CY85A	0.5 g	Yes (2)	No	14
	CY85A	5.0 g	Yes (4)	No	14

was not known.) After the chamber had been flushed, a small payload of 0.5 g was burned and size distributions were made. After a period of about one to two hours a larger payload of the same pyrotechnic was burned. From 10 to 12 March the large payload was either 80 or 160 g (for extinction and mass loading experiment). After 12 March the second payload was always 5 gr and the humidity in the chamber was below about 40% RH.

Size Distributions. Figures 4 and 5 show typical size distributions obtained for the 0.5 g and 5 g burns of CY85A. The stars denote the differential size distribution taken with the mobility analyzer and the diamonds are the cumulative size distribution calculated from the differential size distribution. The symbol R denotes the cumulative size distribution obtained from the five channels of the Royco Optical Particle Counter. The size distributions are shown in both Figures 4 and 5 and are from two data sets taken about 20 minutes apart.

Five different pyrotechnic formulations were tested. They were CY85A (Salty Dog), NWC78, NWC79, NWC164 and LiCl; the latter formulation was specially formulated by NWC for these tests at Calspan's request. The exact composition of the bulk pyrotechnic and the predicted aerosol composition can be found in Hanley et al (1981, 1982). The composition of the first four pyrotechnics are largely NaCl or KCl with some MgO. NWC164 contains a small amount of graphite. The particles resulting from these four formulations deliquesce in the range of about 60 to 80% RH and therefore all size distributions presented for these formulations are truly dry-size, size distributions. LiCl is radically different from the other four formulations in that it starts to take up small amounts of water at very low relative humidities, possibly as low as 11 to 13%. Growth of LiCl at RH below 40% is still relatively small but the size distributions presented for LiCl are not truly dry-size distributions.

The size distributions obtained from CY85A, NWC78, NWC79, and NWC164 for both the 0.5 g and 5 g burns were all very similar to those of CY85A shown in Figure 4 and 5 and therefore will not be shown. The size distribution obtained from LiCl was noticeably different and is compared to the CY85A for 5 g burns in Figure 6. The LiCl appeared to give a significantly better yield in the size range measured.

As the payload of the burn increased there was a shift of the mean size to larger sizes, this is shown in Figure 7 for CY85A burns of 0.5, 5.0, and 160 grams. This result has several important practical implications in regard to the transferability of chamber results to real burns where the payload is much greater and to the optimum method for burning the pyrotechnic. These implications will be discussed in the next section.

In order to obtain more insight into how alteration of the burn might affect the size distribution, it was decided to ventilate the pyrotechnic with compressed air during the burn. The idea was to dilute the recondensing gases so that the particles formed would be small in size. A comparison of a nonventilated burn and ventilated burn of CY85A is shown in Figure 8 and does indicate a slight shift toward smaller sizes. Likewise, a more contained burn was attempted by placing a 6" diameter chimney above the burn. This shifted the size distribution to slightly larger sizes; however, much of the pyrotechnic recondensed onto the chimney which greatly reduced the yield of the burn.

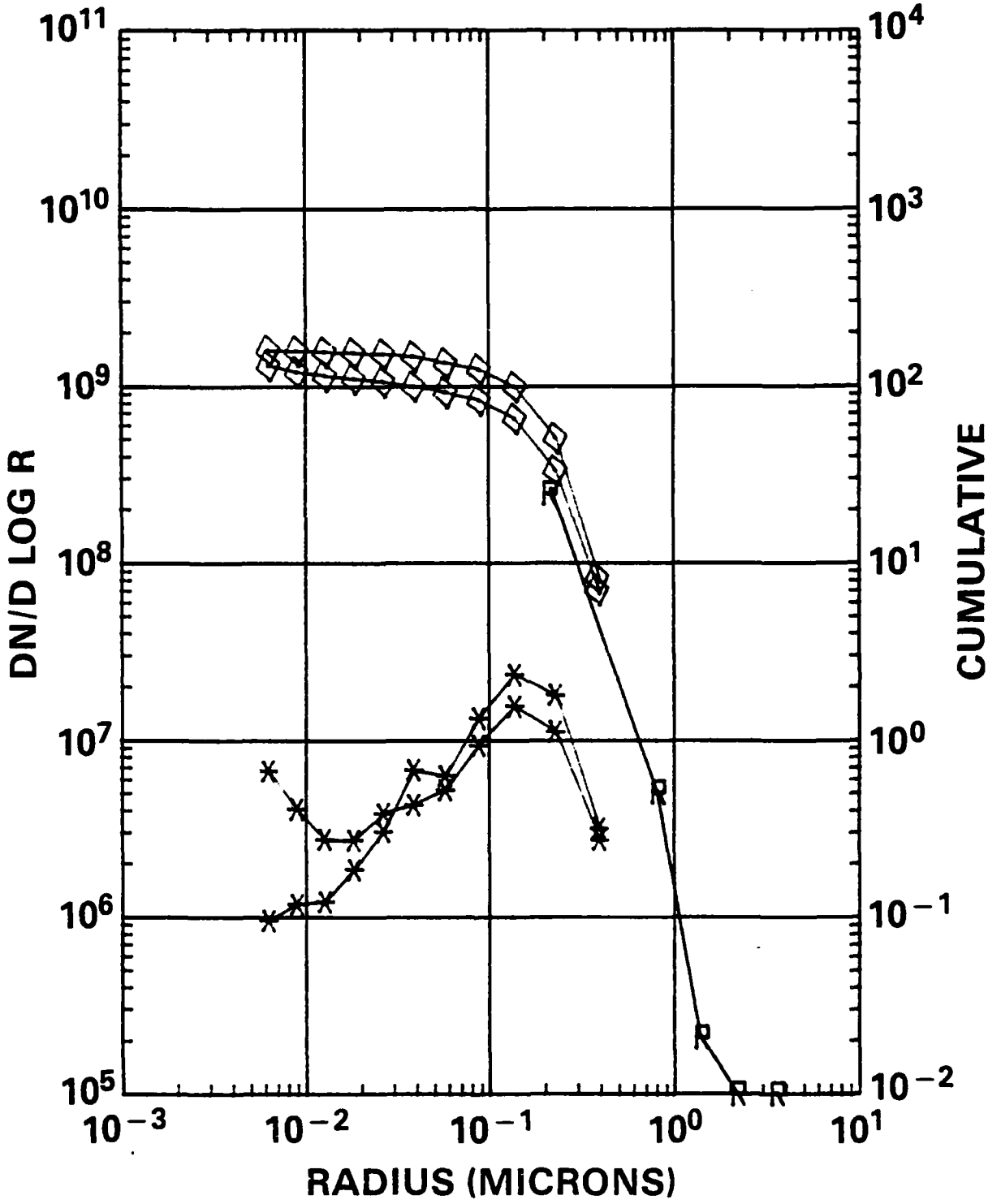

Fig. 4 – Consecutive size distributions from a 0.5 gram CY85A burn

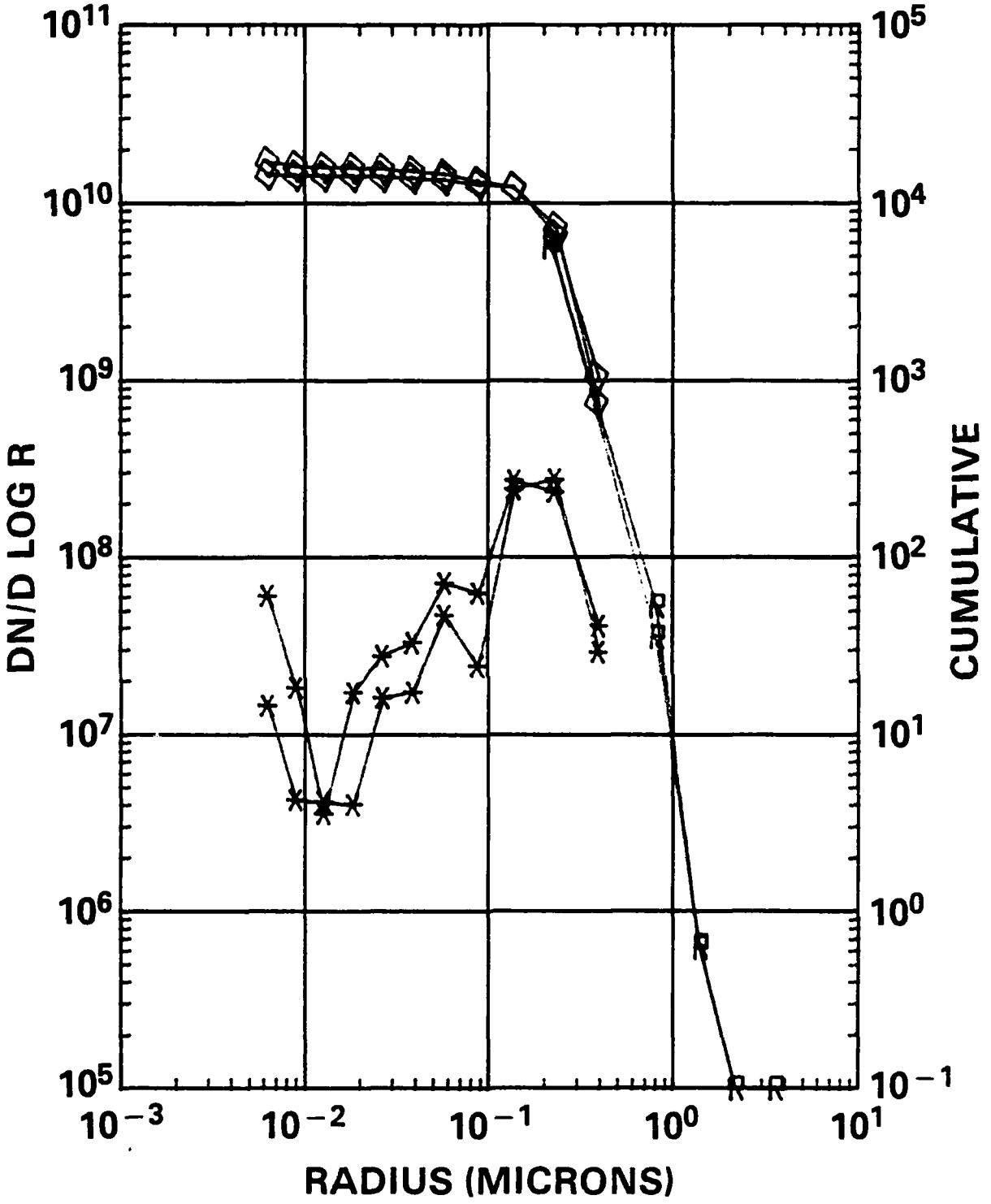

Fig. 5 – Consecutive size distributions from a 5.0 gram CY85A burn

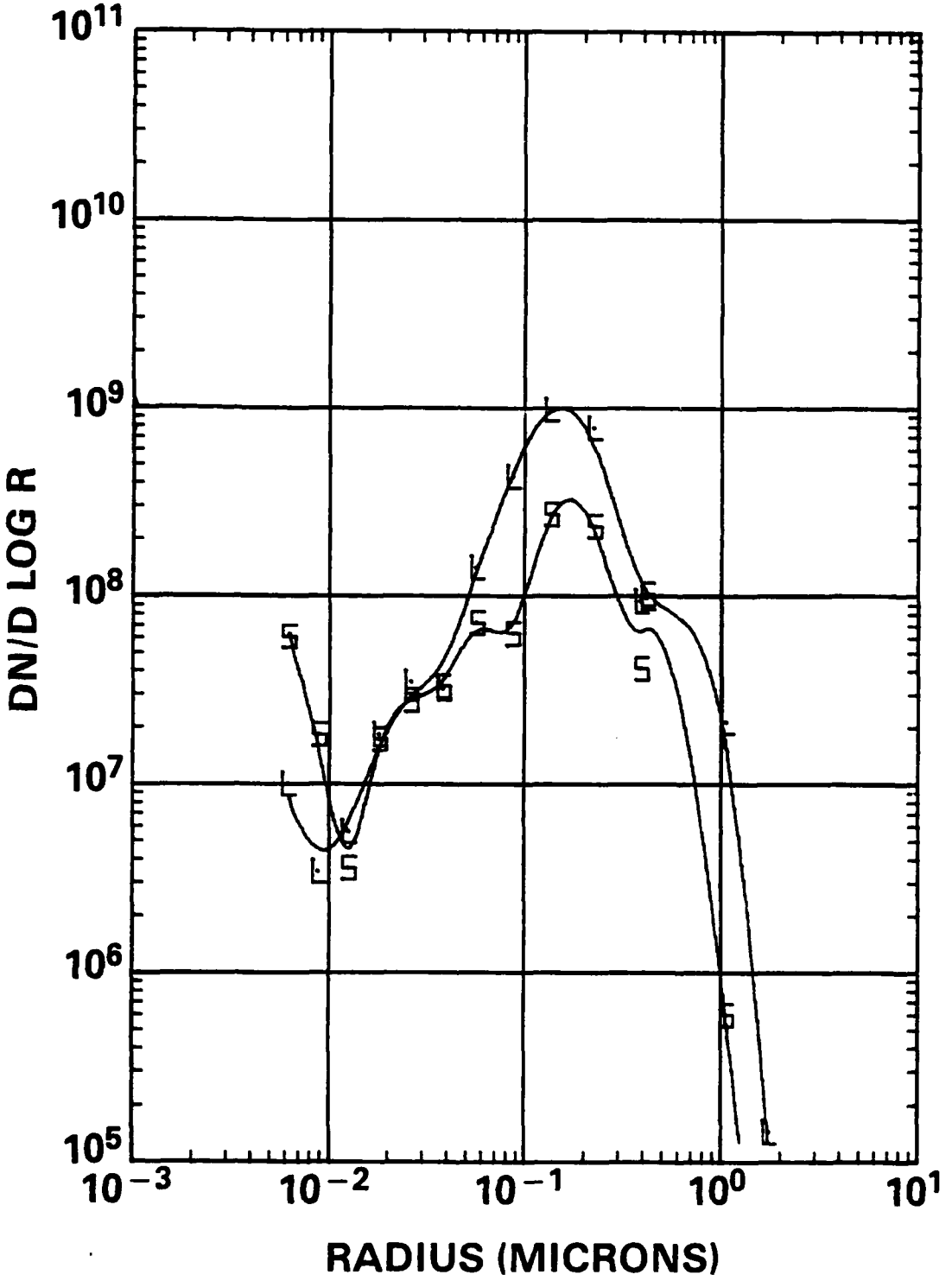

Fig. 6 – Size distributions from 5.0 gram burns of LiCl formulation and CY85A (Salty Dog)

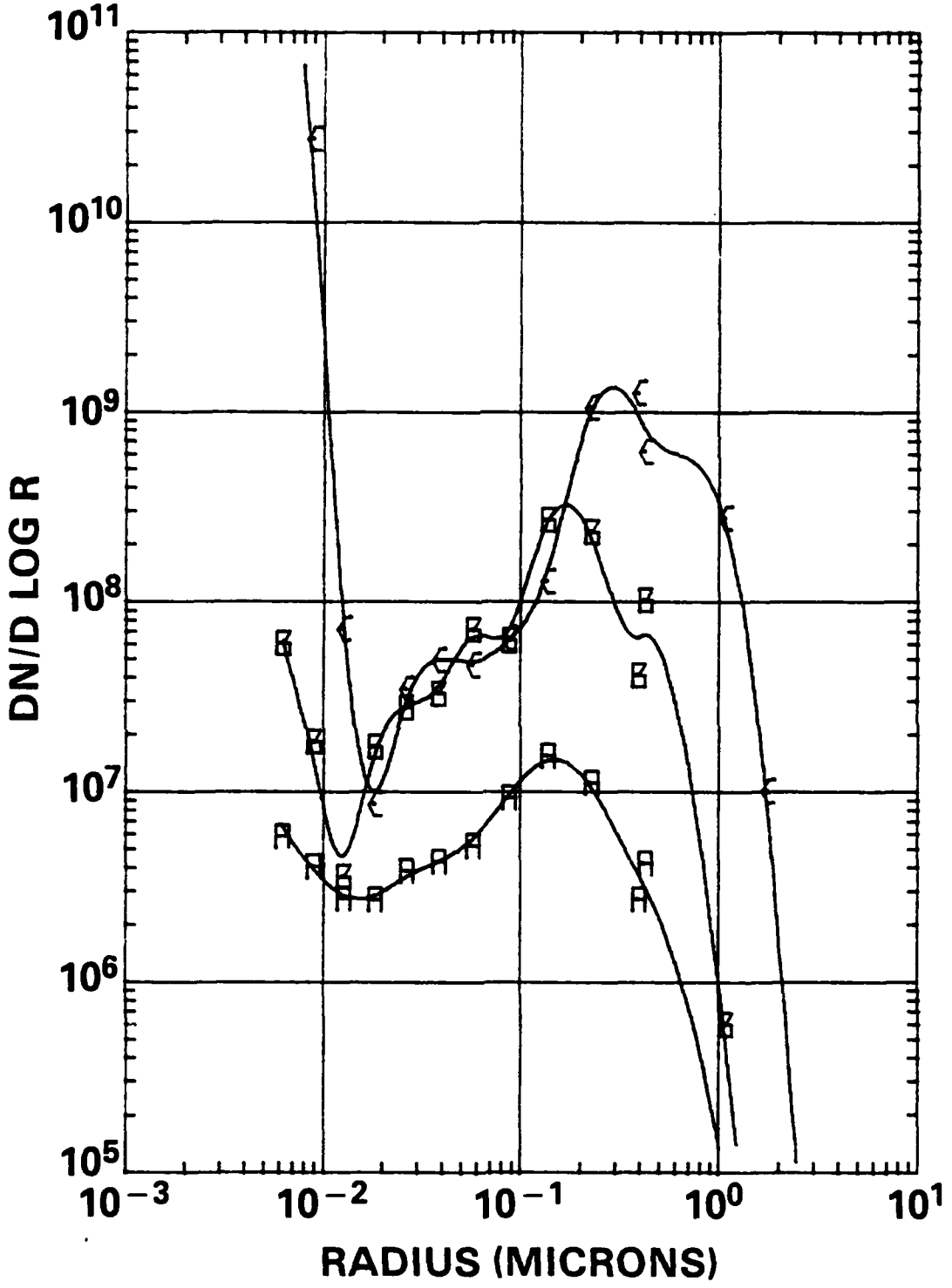

Fig. 7 — Size distributions from 0.5, 5.0 and 160 gram CY85A burns

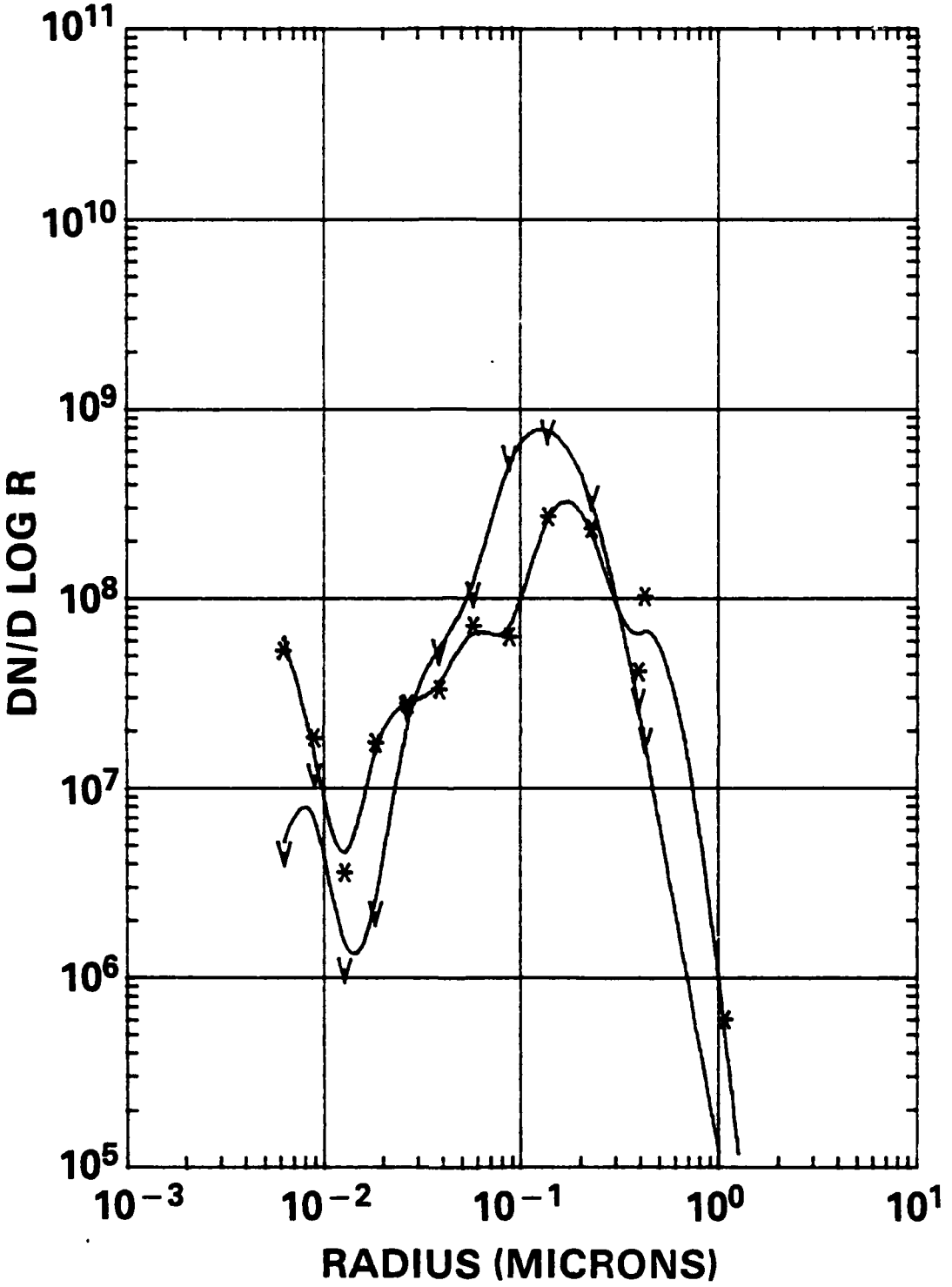

Fig. 8 – The effect of ventilation on a 5.0 gram CY85A burn

The smooth curves through the data points in Figures 6, 7 and 8 were obtained by fitting a least-squares cubic spline to the data points.

Aerosol mass distributions were developed from the combined mobility analyzer and Royco data. The cumulative mass distributions (grams per cc) of Figure 9 represent the burning of 0.5, 5.0 and 160 gram payloads of CY85A, for which a uniform particle density of 2.0 g cm^{-3} was assumed. By further assuming that the aerosol was well mixed throughout the 600 m^3 chamber (the operation of a stirring fan within the chamber gives credence to this assumption), the total airborne masses of 0.179, 3.28 and 147.4 grams are obtained. These correspond to mass yields of 35.8, 65.6 and 92.1 per cent. These values cannot be accepted as valid mass yields because, as stated earlier the dilution system was known to be in error by as much as 40% at the higher dilution ratios. The values are cited here only to indicate the degree of agreement which was obtained between mass calculated from the size distributions and the mass actually burned.

Solubility Data. The method for obtaining the hygroscopicity parameter B^o by measuring the dry size and size at 100% relative humidity was discussed in detail in the second and third sections of this report (Eq. (3)). Particles of known dry size were transmitted from the mobility analyzer to the isothermal haze chamber, where they were allowed to equilibrate at 100% relative humidity before being sized by a Royco optical particle counter whose calibration had been corrected to that for the refractive index of water droplets. The size transmitted could be selected by changing the voltage on the mobility analyzer and the air flows of the sample and sheath air in the analyzer. A voltage of 2500 to 5000 volts (dry radius in the range of 0.15 to 0.30 μm) was usually optimum because in this size range the size distribution is decreasing rapidly with increasing size. This is important because larger particles which are multiply charged may be transmitted along with the more numerous singly charged particles. If the number of particles is decreasing rapidly with increasing size the number of multiply-charged large particles is greatly diminished. In addition to choosing the transmitted size in a region where the size distribution is rapidly decreasing, a correction was made for multiply charged larger particles based upon the size distribution made just prior to the growth measurement. Figure 10 shows a typical result where the solid bar indicates the size range of particles transmitted and the vertical height has no meaning, i.e. dry-size concentration transmitted was not measured. The dotted histogram shows the size distribution of particles at 100% relative humidity and shows that the particles have grown by more than a factor of 5. There are some particles recorded in extreme channels. This is either due to nonuniformity of the particle composition or instrumental limitations; the latter is more likely to be the case.

Figure 10 is for CY85A with 3620 volts on the analyzer and a 5 gram burn. No difference in hygroscopicity was noted between results for 5 g burns and 0.5 g burns.

Unfortunately, no growth data was obtained for LiCl, primarily because the relative humidity necessary to insure dry size is very low (~ 10% RH). The solubilities obtained for the other formulation are the same within the measurement accuracy. The actual values obtained for B^o were: CY85A, 0.28 $\pm$ .05; and NWC78, 0.30 $\pm$ .05; NWC79, 0.36 $\pm$ .05; and NWC164, 0.38 $\pm$ .05. These values are seen to be less than for pure salts. Some typical salts of

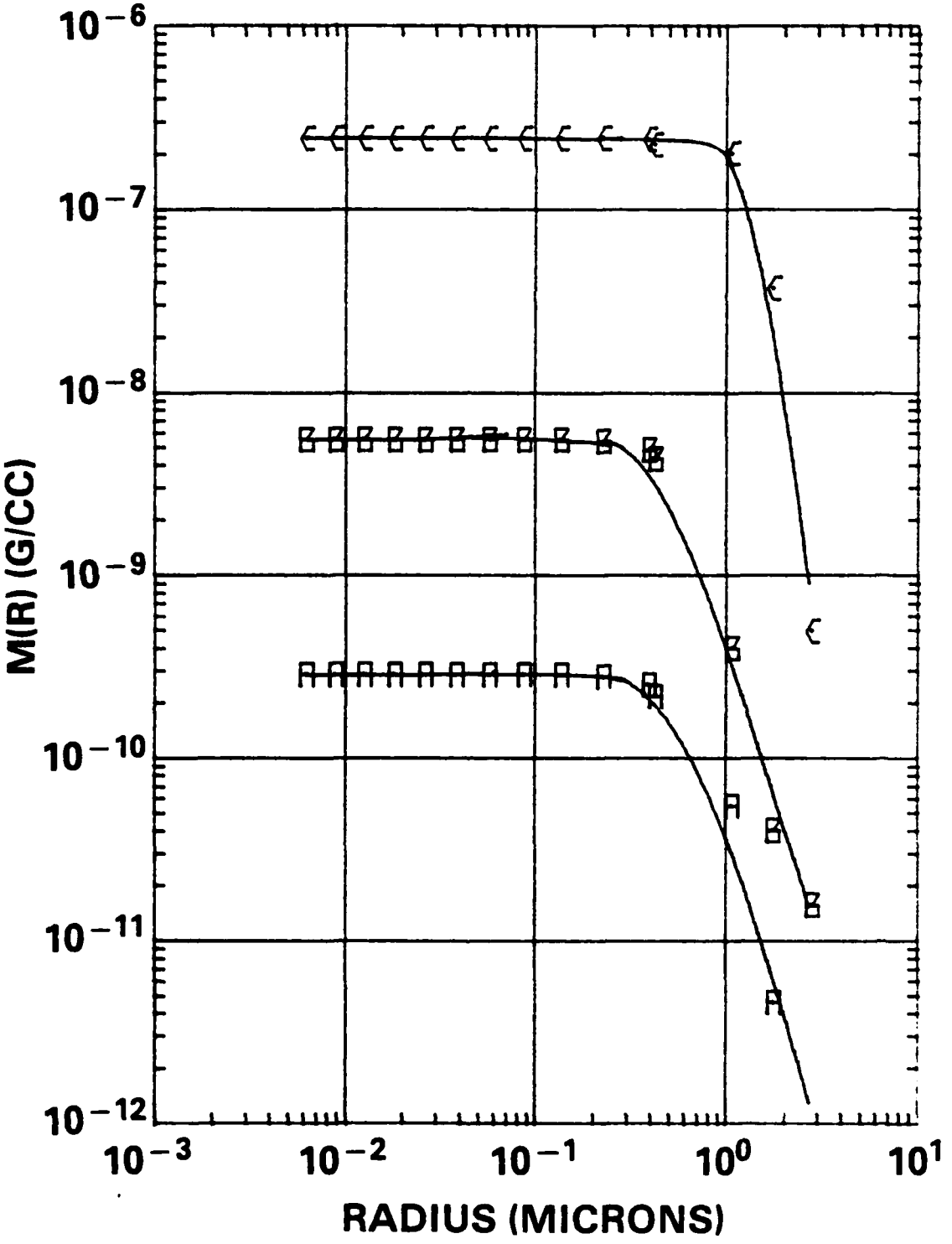

Fig. 9 – Cumulative mass distributions of 0.5, 5.0 and 160 gram CY85A burns

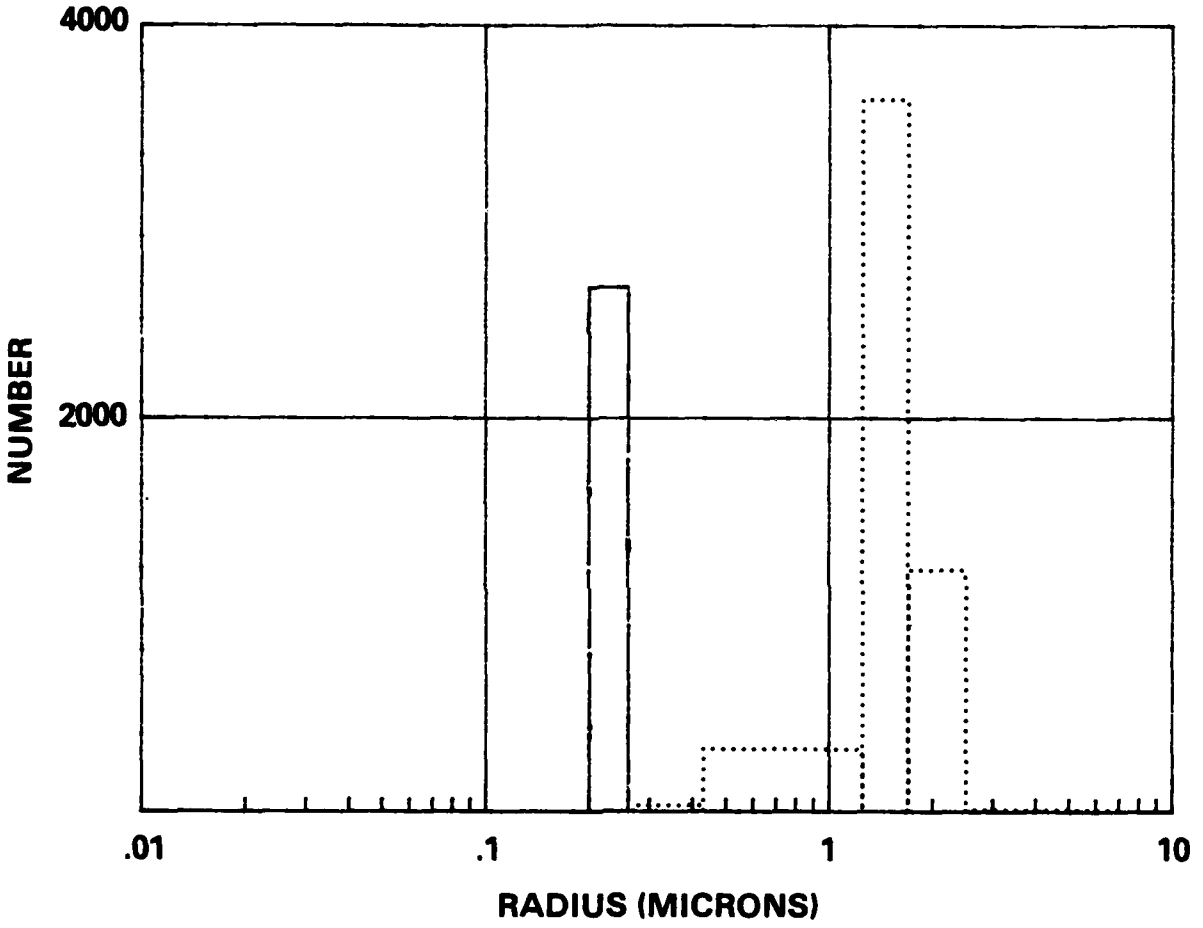

Fig. 10 — The growth of particles from dry to equilibrium size at 100% R.H. from a 5.0 gram CY85A burn

interest have the following approximte values; NaCl, 1.3; $(NH_4)_2SO_4$, 0.6; KCl, .95; LiCl, 1.52.

V. DISCUSSION OF AEROSOL FORMATION AND GROWTH MECHANISMS

The size distribution from the pyrotechnic had a rather well defined peak at a large radius in comparison to that usually found in the atmosphere or that generated by the internal combustion engine. There was a decided shift in the size distribution toward larger sizes when the payload was increased from 5 to 160 grams. Furthermore there was a measurable shift in the size distribution toward smaller sizes when the 5 gram burn was strongly ventilated. A better understanding of the particle formation mechanism may make it possible to optimize the conditions of the burn. Gathman (1982) has shown that the size for maximum extinction for a given payload is about 1 micron for a wavelength of 3.75 μm.

The purpose of this section is to examine aerosol growth mechanisms in connection with the measured size distributions and see if any insight into the physical mechanisms determining the size distribution can be gained.

The two main mechanisms for particle growth are condensational growth by diffusion of vapor to the particle and growth by coagulation of particles. Both of these mechanisms act simultaneously, however it is convenient to look at the two mechanisms separately to get some insight into their relative importance.

Diffusional Growth of Particles. Since oxidizer is built into the pyrotechnic it burns without an external supply of air so there could be a steady flux of vaporized material from the flame without entrainment of air at the bottom of the flame. For purposes of analysis we assume a one-dimensional flame composed entirely of vaporized pyrotechnic molecules of concentration n. It is reasonable to assume that recondensation of the vapor into particles occurs when the vapor is cooled to the boiling point temperature T_v of the solid material of which particles are composed (T_v is about 1700 deg for NaCl and KCl). The concentration of recondensing molecules at that point is approximately

$$n_v = \frac{P}{kT_v} \tag{4}$$

where P is atmospheric pressure. This gives an initial concentration of recondensing molecules of about $5X10^{18}$ cm^{-3}. The saturation ratio with respect to the condensing molecular species can be written as

$$S = \frac{n}{n_s(T)} \tag{5}$$

where $n_s(T)$ is the saturation vapor concentration for the condensing material at a temperature T. The saturation vapor concentration will decrease rapidly as the material cools by radiation, causing a high degree of supersaturation. It is well-known from nucleation theory that the number of particles nucleated depends on the maximum supersaturation attained, i.e., the larger the

maximum S the greater will be the number of particles formed in the recondensation process. In order to calculate S, the rate of cooling must be known as well as the saturation vapor pressure as a function of temperature. Also the time dependence of n must be calculated, taking into consideration the loss of molecules to the newly formed aerosol particles. This is a formidable task requiring a combination of heat transfer and nucleation theory.

A greatly simplified picture which will aid us in understanding the recondensation mechanism can be obtained by estimating the concentration of particles in the condensing zone from the total number in the chamber after dispersion of the aerosol. If the total mass M_t of pyrotechnic is burned in a time t then the rate of vapor production in molecules per unit time is given by

$$R_m = \frac{Av \cdot M_t}{M \cdot t} \tag{6}$$

where Av is Avogadro's number and M is the molecular weight. The outward velocity of the vapor, neglecting convection is

$$v = \frac{R_m}{\text{Area} \cdot n_v} \tag{7}$$

where Area is the area of the burn and n_v is the concentration of molecules given by Eq. (4). If the concentration of particles in the chamber is Z and the volume is V_c, then the concentration of particles in the recondensing zone is just

$$Z' = \frac{(ZV_c) \cdot M \cdot n_v}{Av \cdot M_t} \tag{8}$$

This expression is independent of the area and duration of the burn. It was assumed that the particles Z' move with a velocity v through the recondensing zone.

The experimental data on the concentration of particles Z in the chamber would indicate (using Eq. (8)) that the concentration of particles Z' in the recondensing zone was only about one-fifth as great for the 160 gram burn as for the 5 gram burn (even though the dispersed aerosol concentration were about five times as great). Comparing the 5 gram and 0.5 gram burns indicates that the particle concentration was about the same in these two cases (within the crudeness of this approximation). From this we conclude that the maximum supersaturation and hence rate of cooling achieved in the two smaller payloads were about the same and considerably greater than occurred in the larger burn. This seems entirely reasonable since both radiative and conductive cooling would proceed more rapidly when the surface-to-volume ratio of the burn is larger.

So far we have assumed there exists a well-defined recondensation zone and have said nothing about the rate of recondensation. The concept of a well-defined recondensation zone implies that recondensation occurs before the plume is significantly dispersed. A rough estimate of the velocity from Eq. (7) using visual observation of the duration and area of the five gram burn would indicate the velocity of the vapor flux to be in the range of 200 to 1000 cm per sec. It will be shown that recondensation in the high vapor concentrations given by Eq. (4) occurs on a time scale of order less than a millisecond, implying that most recondensation occurs very close to the burn.

The growth of particles much smaller than the molecular mean-free-path is determined by molecular collision rates, whereas for particles much larger than the mean-free-path the growth is diffusion limited. The growth of pyrotechnic particles is in that difficult region between kinetic theory and diffusion theory. The particle growth equation can be written as

$$r \frac{dr}{dt} = \frac{D' m}{\rho} \left[n - n_s(T) \right] \tag{9}$$

where r is the radius of the particle of density ρ, n is the concentration of condensing molecules of mass m, and D' is the effective diffusion coefficient. The effective diffusion coefficient (see for example, Hoppel, 1975) is a function of radius such that the growth rate goes over to the kinetic theory rate for small particles and to the diffusion-limited case for larger particles. $n_s(T)$ is the equilibrium vapor pressure of the droplet at a temperature T. We assume initially that the particle is cooling rapidly enough that $n_s(T)$ is much less than $n\left[n_s(T) \approx 0\right]$. Surface tension effects have also been neglected.

The radius increases at the expense of vapor molecules so that the rate of decrease of molecular concentrations is

$$\frac{dn}{dt} = -4\pi D' r Z' n + H \tag{10}$$

Where H is the production rate which we take to be zero in the recondensing zone (i.e. the vapor is formed prior to recondensation). The first term is just the rate at which particles diffuse to aerosols of radius r and concentration Z'.

Eliminating time t from Equations (9) and (10) and integrating gives the relationship between the current radius r of the particle and the molecular concentration n

$$r^3 - r_o^3 = \frac{3m}{4\pi\rho Z'} (n_o - n) \tag{11}$$

Eq. (11) is also simply a statement of conservation of mass. If the initial radius r_o is zero and $n_o >> n$, then the final radius is proportional to the initial vapor concentration and inversely proportional to the concentration of particles Z' in the recondensing zone.

$$r_f^3 = \frac{3mn_o}{4\pi\rho Z'}$$

In order to evaluate the growth rate of particles Eqs. (9) and (10) must be solved simultaneously. Combining Eqs. (9) and (10) and setting $r_o = 0$ yields

$$\int_o^r \frac{r\,dr}{1-Q\,r^3} = \frac{D'\,m\,n_o}{\rho} \int_o^t dt \qquad (12)$$

where $Q = \frac{4\,\rho Z'}{3mn_o}$

Integrating Eq. (12) yields

$$t = \frac{\rho\,Q^{-2/3}}{D'\,mn_o}\left[\frac{\pi}{6\sqrt{3}} - \frac{1}{6}\ln\frac{(1-X)^3}{(1+X+X^2)} - \frac{1}{\sqrt{3}}\tan^{-1}\left(\frac{2X+1}{\sqrt{3}}\right)\right] \qquad (13)$$

where $X = Q^{1/3}\,r$

Evaluation of Eq. (13) for conditions expected in the recondensing zone gives growth times of less than a millisecond. For example in the five gram burn Z' was estimated from Eq. (8) to be about 4.5×10^8 per cm^3. In this case the solution of Eq. (13) is shown in Figure 11 where the molecular weight of the condensate was assumed to be 60 and the density 2 g/cm^3. The vapor concentration was assumed to be half that given by Eq. (4) on the assumption that half the vapor resulted from the pyrotechnic binder which is not condensable. From Figure 11 it is seen that the particles grow to a good fraction of their terminal size in a small fraction of a millisecond. If only a fourth of the material is condensible (Calspan gives nominal mass yields of .35 for CY85A) and if the number of particles calculated is increased by a factor of two to account for chamber and measurement losses, then the lower curve of Figure 11 is obtained. As can be seen in Figure 7, the measured size distribution for the 5 gram burn peaked very close to 0.2 micron in fair agreement with the calculation.

The same calculation was done for the 160 gram burn of Figure 7 and the results are shown in Figure 12. In this case Z' calculated from Eq. (8) only a fifth as great as in the case of the 5 gram burn and the final radius was about 0.67 microns. The lower curve is again obtained by assuming that only a fourth of the material is condensible and that the concentration of aerosols in the burn was twice that inferred from the measurements. The measured size distribution for the 160 gram payload peaked in the range of 0.3 to 0.7 microns in agreement with the terminal size calculated in Figure 12.

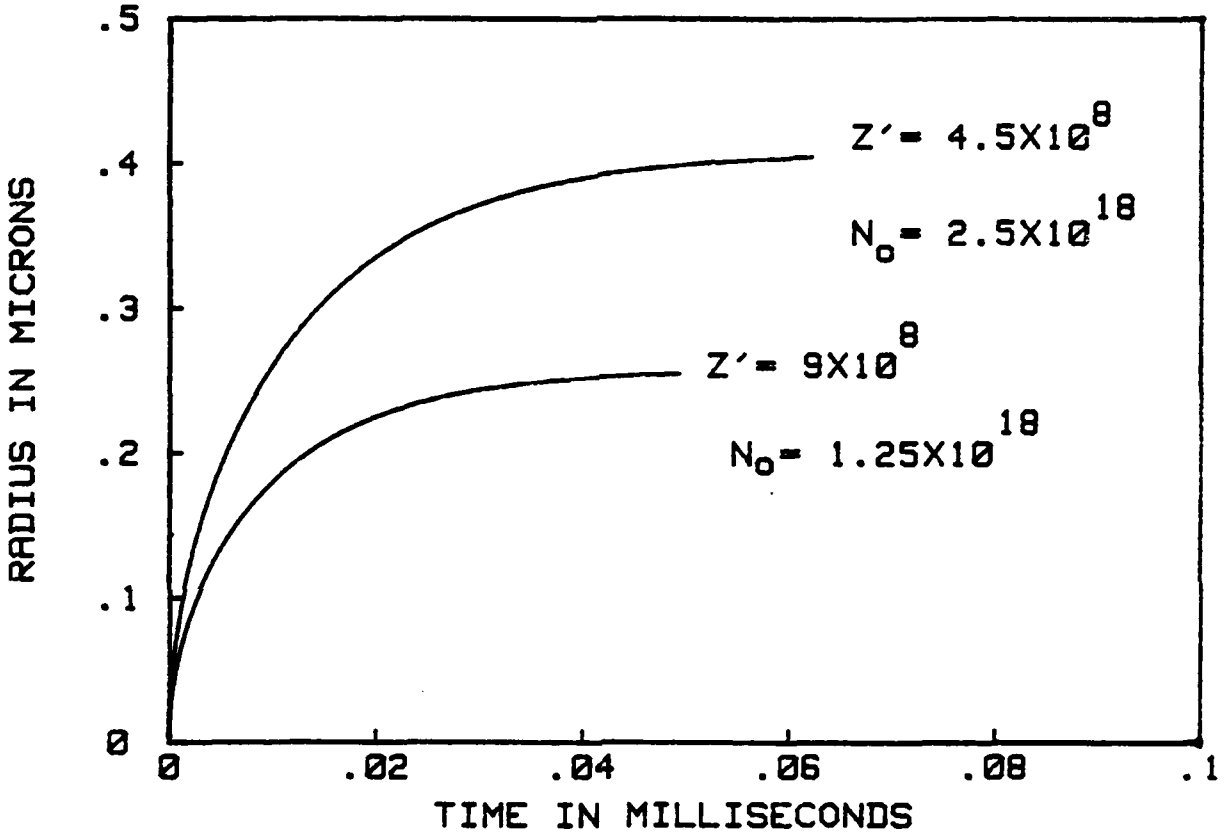

Fig. 11 — The growth of particles in a recondensation process based on estimates of particle and molecular concentrations during a 5.0 gram burn

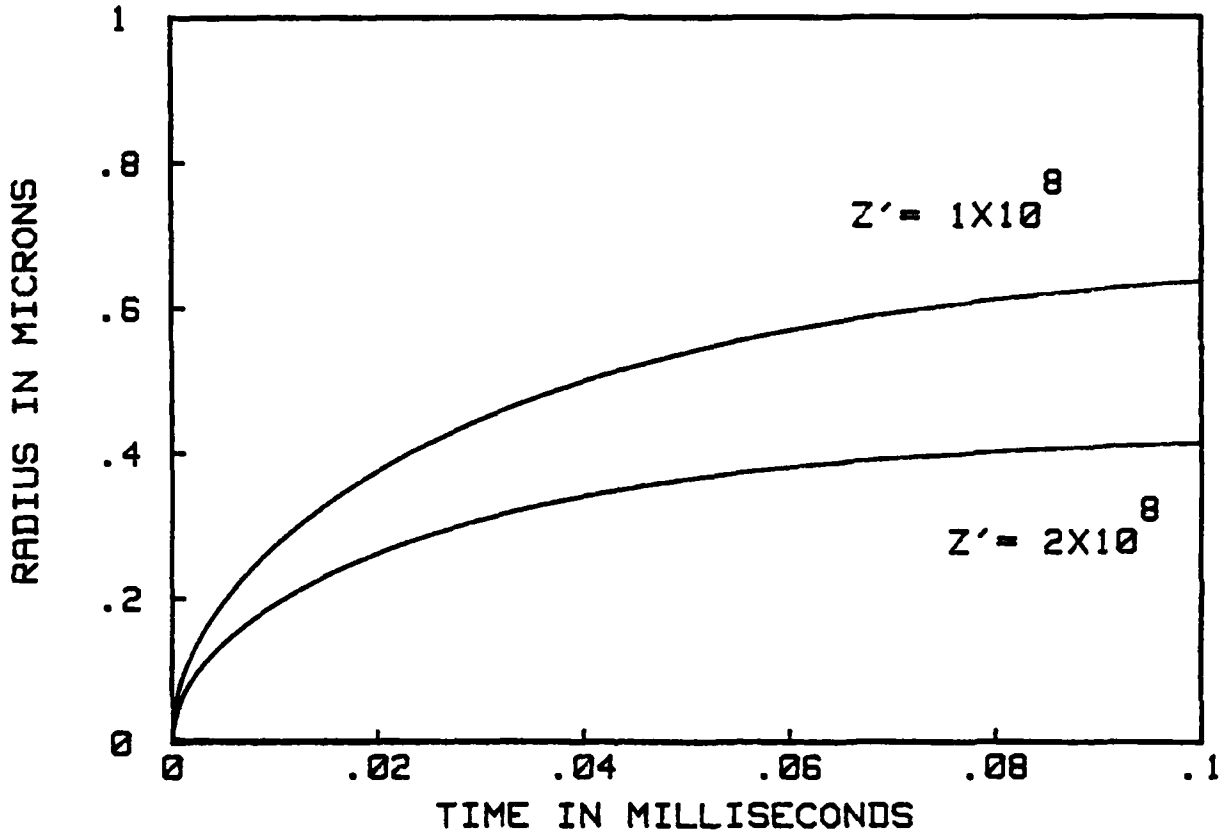

Fig. 12 – The growth of particles in a recondensation process based on estimates of particle and molecular concentrations during a 160 gram burn

The shape of the growth curve (the rapid initial growth compared to later growth) will produce a rather well-defined size. Newly formed particles have a tendency to "catch up" with the larger sized particles when characterized by their radius.

Coagulative Growth of Particles. Shown in Figure 13 is the coagulation coefficient $K(r_1, r_2)$ for particles of radius r_1 and r_2 at normal temperature and pressure. The coagulation coefficient is related to the normalized probability that two particles of radius r_1 and r_2 will coagulate. The probability that two particles of equal size will coagulate is considerably less than the probability that a small particle will collide with a larger particle as indicated by the two curves in Figure 13. The curve labeled K(0.5 μm, r) is the coagulation coefficient for a particle of radius r to coagulate with a particle of radius 0.5 microns.

The rate of decrease of small particles of concentration N as a result of coagulation with larger particles of concentration N_1 can be expressed as

$$\frac{dN_s}{dt} = - K_{s1} N_s N_1$$

If the concentration of large particles is held constant we obtain:

$$\frac{N_s}{N_{so}} = \text{Exp } (-K_{s1} N_1 t)$$

So that the time constant for decay of small particles is

$$T = \frac{1}{K_{s1} N_1}$$

For particles of radius 0.01 micron coagulating with .5 micron particles at the elevated temperature K_{s1} is about 2×10^{-7}. Assuming the maximum particle concentration in the recondensing zone is less than 10^9 cm^{-3} gives a maximum decay time to be about 5 milliseconds. From this we conclude that the coagulation process proceeds somewhat slower than growth by vapor condensation. However the coagulation of smaller particles with larger particles could be important, especially as a mechanism for removing small particles. Coagulation between larger particles is less important on the time scale involved in the aerosol formation process.

In light of the fast condensation rates calculated earlier, the validity of the assumption that the backpressure (equilibrium vapor pressure of the particle) during growth can be ignored is questionable. Only if the growth rate is slower than the cooling rate would $n_r(T)$ in Eqs. (9) and (5) be small compared to n. The driving force for the recondensation is proportional to the gradient (factor in brackets in Eq. (9)) and if the cooling rate is slower than the time required to establish the diffusion gradient then the growth rate will be controlled by the cooling rate.

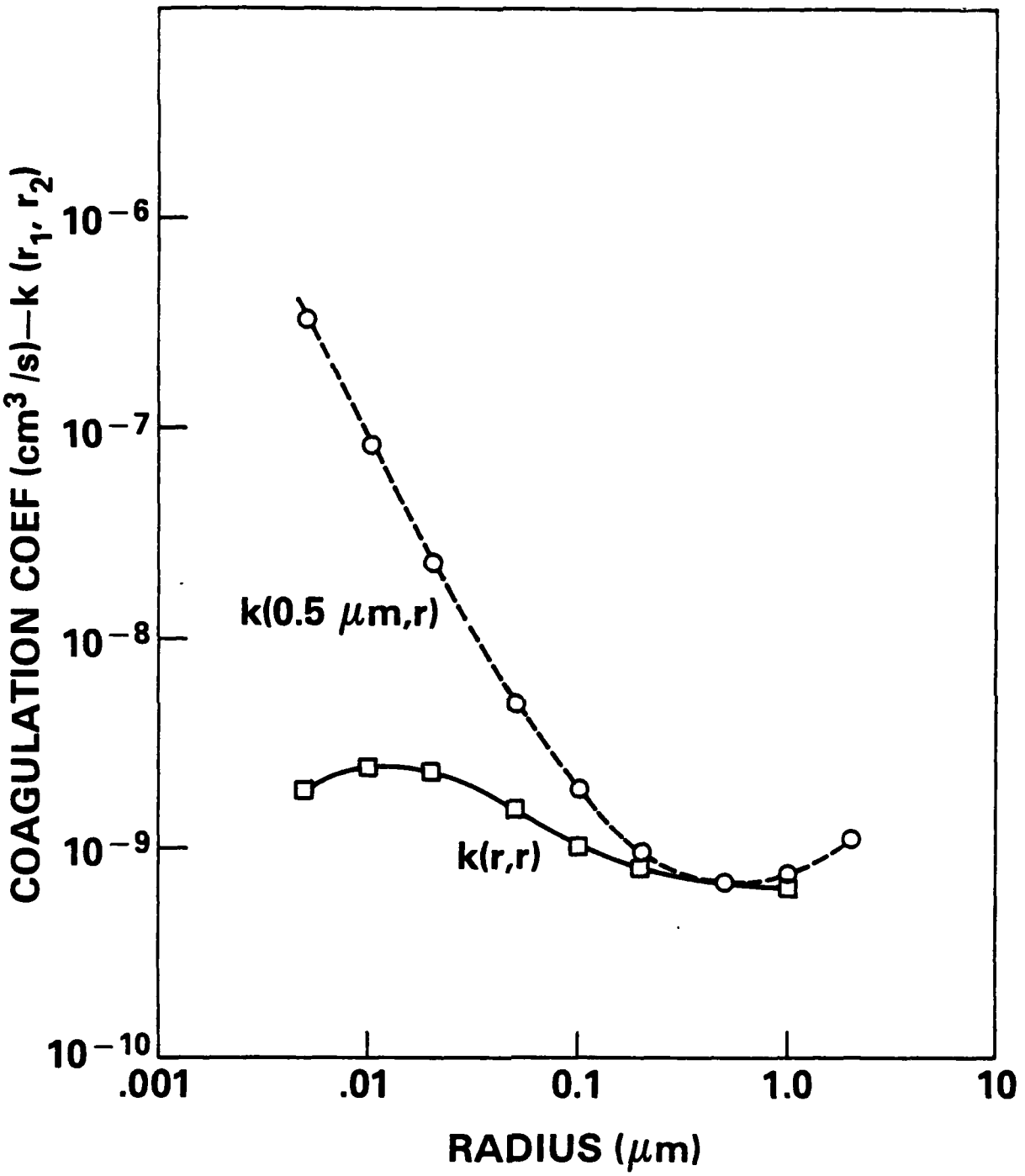

Fig. 13 — The relation between coagulation coefficient and particle radius for same size and 0.5 micron particles

A rough estimate of the radiative cooling rate can be made from the following equation.

$$\frac{dQ}{dt} = \text{Area} \cdot \sigma \varepsilon T^4$$

or for a spherical particle of radius r, density ρ, and specific heat C_v

$$\frac{dT}{dt} = \frac{3 \sigma \varepsilon}{\rho C_v r} T^4$$

Where σ is the Stefan-Boltzmann constant and ε the emissivity. Solving this equation for a particle cooling between 1900K and 1500K yields times of about 0.4 and 4.0 millisec respectively for particles of 0.1 and 1.0 microns. The emissivity was assumed to be 0.5 and the specific heat 0.3 cal g^{-1} deg K^{-1}. This is almost an order of magnitude slower than condensational growth rates calculated earlier. This means that diffusional growth is probably limited by cooling rates, and coagulation between small and large particles becomes more competitive with condensational growth.

The formation of the initial particles was earlier attributed loosely to homogeneous nucleation. The least volatile components (such as MgO) will form particles first and these particles will act as centers of condensation for the more volatile components in the cooler regions of the recondensation zone. If this is the case it might be possible to control the number and size by controlling the least volatile component. Since carrying out these calculations it was learned that, based on unpublished work in the fifties, NWC personnel are of the opinion that most particles are formed by the mechanical breakup of the surface as hot gases bubble through the molten surface. This may be the mechanism by which the initial particles are formed.

It is with some trepidation that we have presented the material in this section, but it is hoped that this discussion will focus attention on the need to understand the aerosol formation mechanism and stimulate further discussion. A better understanding of the physical mechanisms involved will enable development of improved formulations and methods of burning. Unfortunately it is beyond the scope of this year's work to pursue this matter further.

VI. CONCLUSIONS

Measurements of the size distribution of pyrotechnically generated alkali-halide aerosol were made in Calspan's 600 cubic meter environmental chamber for the particle radius range from .007 to 3.5 microns. The pyrotechnics tested were CY85A (salty dog), NWC78, NWC79, NWC164, and a new LiCl formulation. Most of the size distributions were obtained by burning either .5 or 5 grams of the pyrotechnic, however on a few occasions burns of either 80 or 160 grams were made. A summary of the size distributions results are as follows:

1. The size distributions generated by the first four formulations were very similar. Comparisons were made for 0.5 and 5.0 gram payloads. Variations in size between various formulations appeared to be within the variations obtained by repeated payloads of the same formulation. The LiCl formulation generated a size distribution measurably different with more particles at a smaller size.

2. For all payloads most of the particles were larger than 0.1 micron. The amount of mass contained in particles smaller than 0.1 micron is negligible.

3. One of the more interesting results is that the size increased as the payload increased as shown in Figure 7 for CY85A. For the 5 gram burn the size distribution peaked at about 0.2 micron radius whereas for the 160 gram burn the maximum was at about 0.45 microns. (For the mass distribution these peaks occurred at about 0.35 and 1.0 micron respectively.) This result makes it easier to understand why the mean size for a large atmospheric burn (Gathman, et al., 1981) peaked at about one micron (at 90% RH) whereas earlier results in Calspan's chamber (Hanley and Mack, 1980) for a 0.5 gram burn gave almost an order of magnitude smaller particle sizes.

4. Ventilating a 5 gram payload with a steady stream of compressed air during the burn produces a size distribution which is noticeably smaller than that for an unventilated burn.

Measurements of the solubility of individual particles for the various formulations were made using the NRL isothermal haze chamber in conjunction with the mobility analyzer. The results showed that the solubility of CY85A, NWC78, NWC79, and NWC 164 varied only slightly from each other and had a value of about 0.35. The solubility of the particles generated by the LiCl formulation was obviously greater but the measurement failed because it was not possible to reach a low enough humidity to measure the dry size.

New formulations using substances of greater solubility and which deliquesce at lower relative humidities should be tried. The new LiCl formulation by NWC is a significant step in this direction. A major effort for improving the formulation should be made as early in the program as possible. The relative effectiveness of the new formulations should first be compared in chamber tests before employment in more expensive field tests.

We do not believe enough is known about the particle formation mechanism. Gathman (1982) has shown that the optimum size for extinction at various wavelengths can be calculated. It is likely that an improved understanding of the physical mechanism of particle formation would make it possible to modify certain components of the formulation or method of burning to optimize the size distribution for extinction at one or all wavelengths. An experimental effort should be made to determine which of the mechanisms discussed in Section III of this report are most important in determining the size distribution in current formulations. This information would then be available to suggest future improvements.

VII. REFERENCES

Fitzgerald, J. W., W. A. Hoppel, and M. A. Vietti, 1982: "The Size and Scattering Coefficient of Urban Aerosol Particles at Washington, DC as a Function of Relative Humidity". In Press, J. Atmos. Sci.

Gathman, S. G., B. G. Julian, L. A. Mathews, and R. M. McClung, 1981: "Field Experiments with Artificial Aerosols at San Nicolas Island, California". NRL Memorandum Report 4648.

Gathman, S. G., 1982: "On the Relationship of the Dry Size Distribution of Hygroscopic Aerosols to Electromagnetic Radiation Extinction". Proceedings of the Workshop on Hygroscopic Aerosols, Vail, Colorado, In Press.

Hanley, J. T., and E. J. Mack, 1980: "A Laboratory Investigation of Aerosol and Extinction Characteristics for Salty Dog, NWC29 and NWC78 Pyrotechnics". Calspan Report No. 6665-M-1, Calspan Corp., Buffalo, NY, Oct. 1980.

Hanley, J. T., B. J. Wottle, and E. J. Mack, 1981: "Extinction Characteristics of Pyrotechnically-Generated Alkali-Halide Smokes". Calspan Report No. 6855-M-1, Calspan Corp., Buffalo, NY, Dec. 1981.

Hanley, J. T., 1982: "Joint Chamber Tests of NWC Smokes, 8-19 March 1982". In Press.

Hoppel, W. A., 1975: "Growth of Condensation Nuclei by Heteromolecular Condensation". J. Rech. Atmos. IX, pp 167-180.

Hoppel, W. A., 1981: "Measurement of the Size Distribution and Solubility of Submicron Particles". In Atmospheric Aerosols: Their Formation, Optical Properties and Effects. Spectrom Press, Hampton, VA.

Hoppel, W. A. and T. A. Wojchiechowski, 1981: "Measurement of the Size Distribution and Solubility of Salty Dog Pyrotechnic". NRL Memorandum Report No. 4578.